2000

Effects of Evolving Surface Contamination on Spacecraft Charging

W. Y. Chang

JR Dennison
Utah State University

Jason Kite

R. E. Davies

Recommended Citation

W.Y. Chang, JR Dennison, Jason Kite and R.E. Davies, "Effects of Evolving Surface Contamination on Spacecraft Charging," Paper AIAA-2000-0868, Proceedings of the 38th American Institute of Aeronautics and Astronomics Meeting on Aerospace Sciences, (Reno, NV, 2000). Paper received Certificate of Merit by the AIAA Plasmadynamics and Lasers Technical Committee for Best Paper of 2000.

W.Y. Chang, J.R. Dennison, Jason Kite and R.E. Davies, "Effects of Evolving Surface Contamination on Spacecraft Charging," Paper AIAA-2000-0868, *Proceedings of the 38th American Institute of Aeronautics and Astronautics Meeting on Aerospace Sciences*, (Reno, NV, 2000). DOI: 10.2514/6.2000-868

AIAA-2000-0868

EFFECTS OF EVOLVING SURFACE CONTAMINATION ON SPACECRAFT CHARGING

W.Y. Chang, J.R. Dennison, Jason Kite and R.E. Davies
Utah State University, Logan, UT 84322-4415

ABSTRACT

The effects of evolving surface contamination on spacecraft charging have been investigated through (i) ground-based measurements of the change in electron emission properties of a conducting surface undergoing contamination and (ii) modeling of the charging of such surfaces using the NASCAP code. Specifically, we studied a Au surface as adsorbed species were removed and a very thin disordered carbon film was deposited as a result of exposure to an intense, normal incidence electron beam. As a result of this contamination, we found an ~50% decrease in secondary electron yield and an ~20% reduction in backscattered yield. The type and rates of contamination observed are similar to those encountered by operational spacecraft. Charging potentials of an isolated panel of the material were determined under both sunlit and eclipse conditions in geosynchronous orbits for typical and extreme environments. In all environments studied, just monolayers of contamination lead to predictions of an abrupt threshold effect for spacecraft charging; panels that charged to small positive values when uncontaminated developed kilovolt negative potentials. The relative effect of NASCAP parameters for modeling secondary and backscattered electron emission and plasma electron distributions were also investigated. We conclude that surface contamination must be considered to avoid the serious detrimental effects associated with severe spacecraft charging.

INTRODUCTION

Spacecraft charging, due primarily to secondary, backscattered, and photo-induced electron emission, is known to produce many of the spacecraft system anomalies, components failures, and even complete satellite failures attributed to the natural space environment [*Hastings, 1996; Leach , 1995; Garrett, 1981*]. Deleterious effects of spacecraft charging have occurred in all near Earth environments; therefore, spacecraft charging must be considered a serious issue for all earth satellites. To allow spacecraft designers to accommodate or mitigate spacecraft charging effects, NASA has developed an extensive methodology [*Herr 1994*]; central to this is a set of engineering tools (*e.g.*, NASCAP/LEO, NASCA/GEO and POLAR) designed to model the spacecraft environment, predict detrimental charging effects, and determine how these effects interfere with mission goals and objectives [*NASCAP, 1999; Mandel 1993*]. The tools model electronic properties of spacecraft materials and material response to charge-inducing environmental electron, ion, and photon fluxes [*Garret 1978, 1981; Katz 1977,1986; Mandell 1993*]. As with many NASA strategies, the rationale is that extensive, accurate pre-flight modeling of these effects during the spacecraft design stage will provide an accurate, cost-effective way to address spacecraft charging.

Charging models require as input the electronic properties of the component materials of a given spacecraft. Critical to the accuracy of these models are estimates of the secondary electron (SE) and backscattered electron (BSE) yields of the materials. The SE and BSE yields, δ and η, are the number of low and high energy emitted electrons per incident particle, respectively. Because emission of low energy SE is primarily a surface phenomenon, SE yields are extremely sensitive to the presence of surface contaminants. Thus, the addition or removal of surface contamination, even at monolayer thicknesses, can substantially alter the SE yield.

Studies from NASA's Long Duration Exposure Facility (LDEF) have established conclusively that spacecraft surfaces can and generally do undergo significant evolution during their operational lifetime [*Crutcher, 1991a*]. Deposition and removal of contaminants can occur as a result of, for example, preferential adsorption of gases on cooler surfaces, the collection of ionized gases on negatively charged surfaces, atomic-oxygen-induced oxidation, photodissociation under vacuum uv bombardment, and electron- or ion-induced desorption. Therefore, as spacecraft surfaces evolve during the mission due to interactions with the environment, so too do their electron emission characteristics and, consequently, the spacecraft's susceptibility to significant charging in a given environment.

DESCRIPTION OF STUDY

The purpose of the present study is to investigate the effects of contamination on SE and BSE emission

from representative spacecraft materials and to determine the extent to which these effects might alter a spacecraft's charging behavior. A preliminary study of this problem found that for a particular oxidized Al surface the SE yield decreased by more than a factor of 2.3 during surface evolution representative of that experienced by typical spacecraft materials [*Davies, 1997*]. Because the most troublesome spacecraft potentials are negative, the reduction of a surface's SE yield was expected to translate into increased spacecraft-to-plasma charging levels for a given set of environmental conditions. However, this initial study was unable to model spacecraft charging since changes in the SE yield were measured for only a limited range of incident electron energies.

In the present study, we report on our results for another surface, which is also representative of evolution of electronic materials properties that may be encountered on real spacecraft. Polycrystalline Au samples were subjected to relatively intense electron beams for prolonged periods of time. In our studies of both Au and Al/Al_2O_3 [*Davies, 1997*] surfaces, electron bombardment served to stimulate a number of surface effects, which are similar to those that can occur aboard operating spacecraft. Initial electron bombardment rapidly removed surface contamination. A disordered carbon film was deposited through electron stimulated adsorption over a longer time period.

The relevance of our experimental results to spacecraft charging modeling relies on the applicability of the laboratory conditions to those of an operational spacecraft; specifically we need to consider conditions of ambient gas pressure, contamination species and deposition or removal rate, and incident electron energies and currents densities. The vacuum and contaminant levels employed are typical of the microenvironment in close proximity to operating spacecraft in low-Earth orbit [*Davies, 1997*]. Similar adsorbed species or oxide layers and carbon deposition or organic film contamination are commonly found for operational spacecraft. Rates of contaminant deposition and removal observed in this investigation are representative of those recorded aboard LDEF [*Crutcher, 1991b*]. Incident electron energies of 300 eV to 3000 eV employed in this study are typical of the higher energy populations in many plasma environments.

The mechanisms responsible for the sample surface modifications in our ground-based simulations—namely, the electron-beam-induced desorption of weakly bound contamination layers and deposition of carbon—may not be the most important mechanisms in the space environment, because of the lower electron fluxes in the space environment [*Davies, 1997; Hardy, 1985*]. The beam current densities used in our laboratory simulation ($\sim 10^{-4}$ A/cm^{-2}) are approximately five to six orders of magnitude greater than those of the representative orbital environments considered in this study ($\sim 10^{-9}$ to 10^{-10} A/cm^{-2}). However, there are numerous other mechanisms that produce similar surface modifications in the space environment that can potentially result in similar contamination-induced changes in spacecraft charging. Photodissociation of contaminants under vacuum uv bombardment, ion-induced desorption, and attack by atomic oxygen are all ubiquitous mechanisms that remove material. Deposition can result from preferential adsorption of gases on cooler surfaces, outgassing of material (particularly organics), the collection of ionized contaminants on negatively charged surfaces, or atomic oxygen oxidation. The specific process of surface modification is not essential; it is the magnitude of the modification that is important in determining the SE and BSE emission evolution of a surface and the resulting evolution in spacecraft charging.

EXPERIMENT

A 1 cm x 1 cm x 120 μm high purity (4N) polycrystalline Au foil was chemically cleaned and mounted on a Rh plated Cu sample stage. *Ex situ* STM and SEM measurements determined an rms surface roughness of .20 nm over a ~2 mm^2 area typical of our electron beam [*Chang, 2000*]. The sample was placed in a UHV chamber (10^{-10} Torr base pressure and 10^{-9} Torr operating pressures), annealed at ~175 °C for ~ 48 hrs, and then periodically ion sputtered with 500 eV Ar ions with a fluence of ~5 mC/cm^{-2} to prepare a clean surface. A standard Peirce-type electron gun with a tungsten filament was used at normal incidence, operating at beam energies of 300 eV to 3000 eV. The sample remained at room temperature throughout the measurements. A complete description of the apparatus and methods employed is given by Davies [*1996, 1999*].

To establish a baseline for the contamination studies, the total SE yield (emission energies up to 50 eV), δ^*, and the total backscattered yield (emission energies of 50 eV to the incident beam energy), η, for a clean, freshly sputtered Au surface were measured for incident energies ranging from 300 eV to 3000 eV. A low electron current density (~6 nA/cm^{-2}) was used to reduce the rate of electron-stimulated adsorption of carbon for negligible deposition during the measurements. The yields were determined from direct measurements of the net current flowing from the sample to ground and the net current returning to tertiary collectors adjacent to the sample with both the sample and tertiary collectors biased alternately to 0 V and +50 V. Details of the method are given by Davies

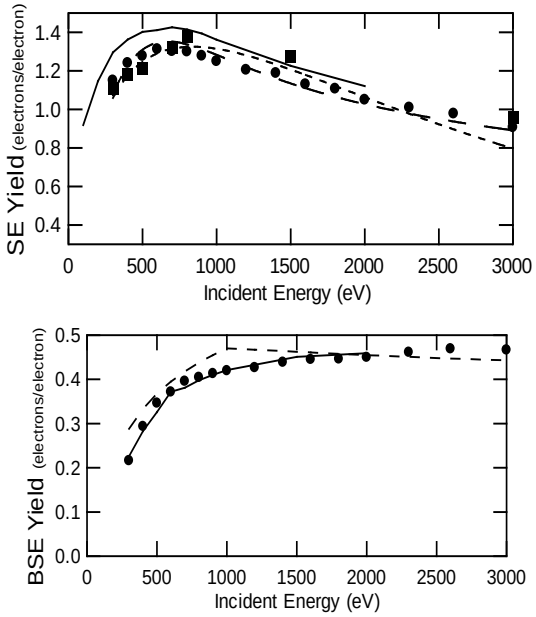

Figure 1. (a) SE and (b) BSE yields vs incident beam energy for a clean polycrystalline Au surface. Measured data, using a low density electron beam and corrected for the systematic ' error, are shown in (a) and (b) as circles; uncertainties are less than the size of the symbols. Values of the fitting parameters $*_{Au}(E_o)$ from Eq. 1 are shown in (a) as squares. The results of Thomas and Pattinson [*1970*] are shown as solid lines in (a) and (b) for comparison. Fits to the *(E) data using the NASCAP model [*Katz, 1977*] of Eq. 2 (dashed) and the Sternglass model [*1957*] of Eq. 3d (dotted) are shown in (a). A fit for the NASCAP model [*Katz, 1977*] of 0(E) using Eq. 4 is shown as a dashed line in (b).

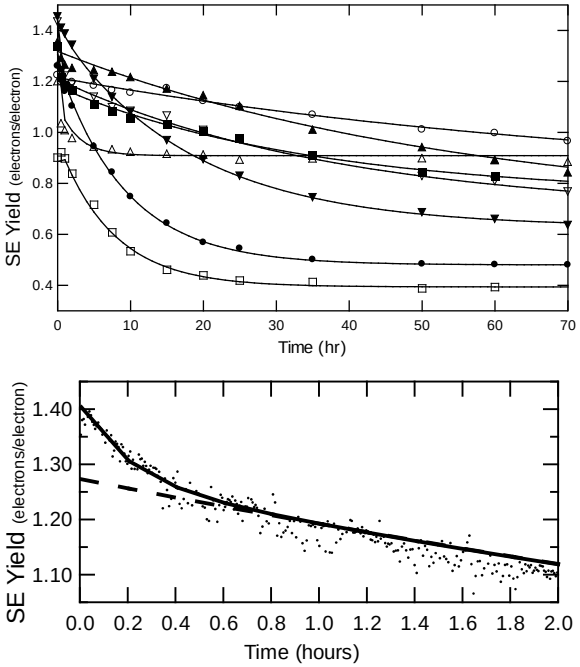

Figure 2. (a) Time evolution of SE yield for a polycrystalline Au surface for incident beam energies from 300 eV to 3000 eV. Curves are fits based on the model of Eq. 1. Symbols indicate incident energies: Î-300 eV; ■-400 eV; ○-500 eV; «-600 eV; •-700 eV; – -800 eV; ●-1500 eV; □-3000 eV. (b) Detail of the initial time evolution of SE yield at 1500 eV. The solid line indicates the fit based on Eq. 1, while difference between the solid and dashed lines shows the contributions to the curve from rapid desorption of adsorbed species [term (i) of Eq. 1].

[*1996*] and similar techniques are described by, *e.g.*, Dionne [*1973*] and Darlington [*1972*].

Our measurements of * and 0 are compared with those of Thomas and Pattinson [*1970*] in Fig. 1. Relative uncertainties in our yields were typically ~0.5%. Agreement between our measurements and those of Thomas and Pattinson over their measured range of 400 eV to 1500 eV was within the relative uncertainty for the total yield F/*+0. However, our method suffered from a systematic error due to over collection of the sample return current by the tertiary collectors when biased to +50 V [*Davies, 1999*]. This resulted in underestimation of the absolute values of * by 25% and an overestimation of the absolute value of 0 of >40%. The systematic error is independent of incident energy, resulting rather from the geometry of the collecting surfaces and the surrounding vacuum chamber. All data presented here, including that in Fig. 1, have been corrected for this effect by a single normalization constant '=0.100"0.001 determined by comparison of our measurements of 0 for clean Au to that measured by Thomas and Pattinson at 400 eV to 1500 eV [see Fig. 1(b)]. The corrected yields have a reproducibility of .0.5% and absolute accuracy of ~1%.

Surface modification was accomplished using a relatively high intensity electron beam at normal incidence with a constant incident electron sample current of 2.00"0.05 :A for prolonged periods of time. The beam diameter decreased from 1.7 mm FWHM to 1.3 mm FWHM with increasing beam energy over this 300 eV to 3000 eV range, corresponding to an decrease in electron current density from ~90 :Acm^{-2} to ~140 :Acm^{-2}. Based on comparison with the current densities in our previous study [*Davies, 1997*], on optical transmission of disordered carbon films [*Dennison, 1985*], on *in situ* low resolution Auger electron spectroscopy, and on analysis the time evolution of * and 0 presented below, the order of magnitude of the deposition rate of the carbon film was estimated to be ~10^{-2} nmhr^{-1} or ~½ monolayer per day.

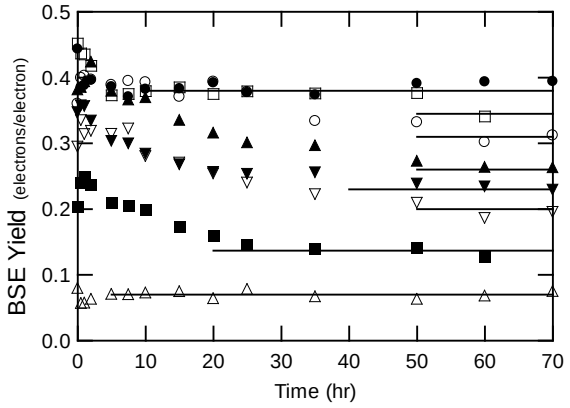

Figure 3 Time evolution of BSE yield for a polycrystalline Au surface. Solid lines indicate the saturated values of 0 after long exposure. Symbols indicate incident energies: Î-300 eV; ■-400 eV; ○-500 eV; «-600 eV; • -700 eV; – -800 eV; ●-1500 eV; □-3000 eV

The SE and BSE yields were measured using the same high intensity electron beam at a fixed incident energy as a function of surface contamination (*i.e.*, high intensity beam exposure time). Data were taken at 35 s intervals for periods of 70 hrs. Figures 2 and 3 show yield profiles for the time evolution of * and 0 due to surface modification at incident energies ranging from 300 eV to 3000 eV, respectively.

ANALYSIS AND RESULTS

Model of the time evolution of SE Total Yield

A simple model of the evolution of SE total yield due to contamination was developed by Davies and Dennison [*1997*], and is applied here as well:

$$\delta_{tot}(t) = (\delta_{WB} - \delta_{Au}) \cdot e^{-\alpha t} + B \cdot e^{-\beta t} \\ \delta_{Au} \cdot e^{-\gamma t} + \delta_C \cdot (1 - e^{-\gamma t}) \qquad (1)$$

The terms on the right hand side of this expression are interpreted as contributions to the total time-dependant SE total yield $*_{tot}(t)$, from (i) the weakly bound, physisorbed contaminants $[(*_{WB}-*_{Au})e^{-"t}]$, (ii) the strongly bound, chemisorbed contaminants $[Be^{-\$t}]$, (iii) the clean bulk substrate $[*_{Au}e^{-(t}]$, and (iv) the deposited contaminants $[*_C(1-e^{-(t})]$. The energy-dependant

Table 1. Values for parameters in Eq. (1) for fit of 1500 eV incident energy data in Fig. 2

Parameter	Value	Error
$*_{Au}$	1.27	1%
$*_C$	0.48	2%
$*_{WB}$	1.41	5%
1/", min	13	20%
1/(, hr	9	10%

parameters $*_{Au}$ and $*_C$ are the SE yields for the clean bulk substrate material and the bulk yield for deposited surface contamination, respectively; for this study, these are for clean Au and bulk disordered C. $*_{WB}$ and B model the SE yields and initial (t=0) fractional coverage of the weakly and strongly bound contaminants, respectively. ", $, and (are rate constants for desorption of weakly bound contaminants, strongly bound contamination, and deposition of contaminants, respectively.

Fits to our data using this model are shown in Fig. 2. Representative values of the full set of fitting parameters at 1500 eV incident energy are given in Table 1. The results for $*_{Au}$ for term (iii) from the fits to Eq. 1 are shown in Fig. 1 and are in very good agreement with our independent measurements of clean Au surfaces and the results of Thomas and Pattinson [*1970*].

Contamination modeled in term (iv) results from another well-known electron beam effect [*Hiller, 1948; Ura, 1993*]–the electron stimulated adsorption of disordered carbon resulting from the cracking of hydrocarbons deposited on the surface from the residual gas in the vacuum by energetic incident electrons [*Hren, 1979; van Oostrom, 1979*]. The process is commonly encountered in high electron current density applications such as electron microscopy, electron arch welding and discharge, and vacuum tube technology [*Thong, 1993; Reimer, 1993*] The results for $*_C$ for term (iv)--the long exposure time limit for SE yield--are consistent with values typical of disordered C.

It should be noted that carbon can be found in many different forms, with different structures and widely varying electronic properties [*Dennison, 1997*], including secondary electron yields [*Farhang, 1993*]. As shown in Fig. 4, the results of this study for SE yield are more similar to carbon black (presumably highly disordered nanocrystalline turbostatic carbon) than to Aquadag (microcrystalline graphite). This is consistent with limited studies of the structure of electron stimulated adsorption of carbon [*Hren, 1979*]. Since

Table 1. Values for parameters in Eq. (1) for fit of 1500 eV incident energy data in Fig. 2

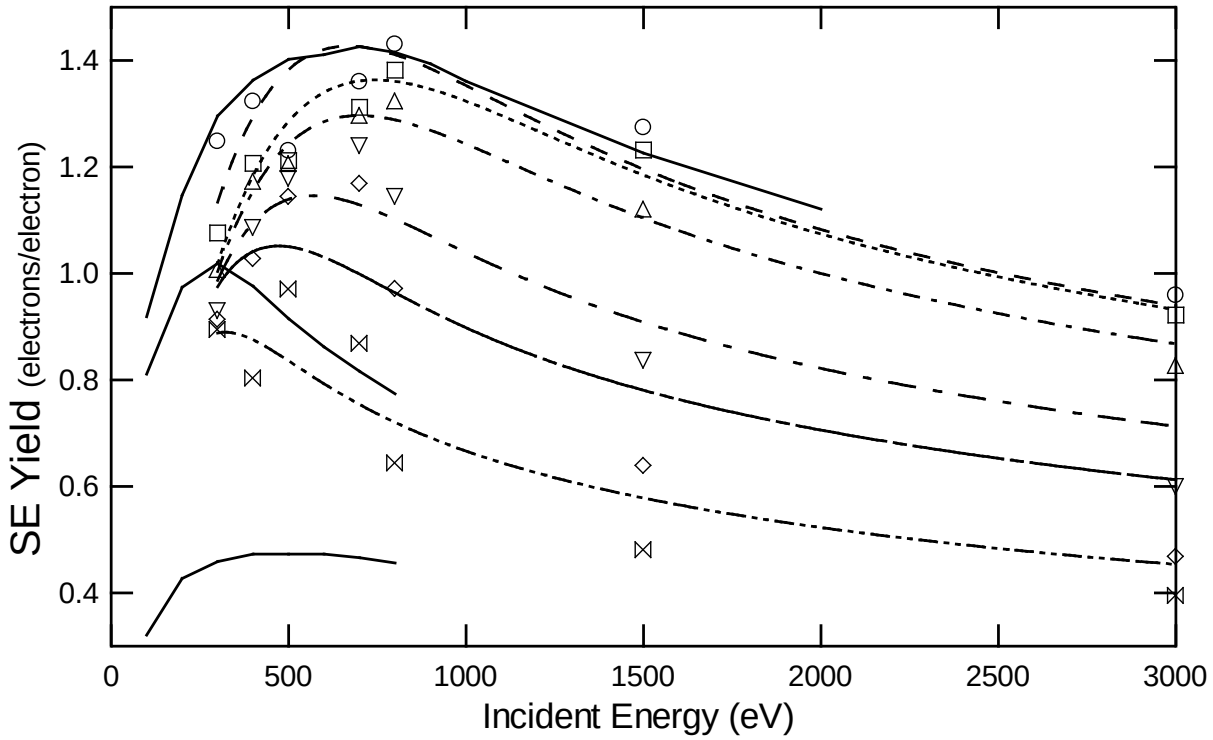

Figure 4. SE emission curves of Au as a function of incident energy for electron beam exposures of 0 hr to 70 hr. Data are from Fig. 2. Dashed curves are fits to the data using the NASCAP model [*Katz, 1986*] of Eq. 3d for various exposure times: ○-0 hr; □-0.5 hr; ª-2 hrs; «-7.5 hrs; •-15 hrs; ®-70 hrs. Solid curves are yield curves for clean Au [*Thomas, 1970*] (top), carbon black [*Bruning, 1938*] (middle), and microcrystalline graphite [*Bruning, 1938*] (bottom), respectively.

disordered C has one of lowest SE yields of any material, C contamination is much more likely to lead to severe negative charging. Highly disordered carbon has even lower SE and BSE yields than the yield observed in this study, and presumably an even more pronounced effect on spacecraft charging. The ubiquitous nature of C contamination, and organic film contamination that has similar effects on SE and BSE yields, is particularly troubling.

The deposition rate of disordered carbon has been estimated as 0.4 nm⇕hr^{-1} to 0.03 nm⇕hr^{-1} assuming the deposition of a carbon film thickness of one inelastic electron mean free path in a time 1/(. In the energy range of our measurements, the inelastic electron mean free path of disordered carbon increases from ~1 nm at 300 eV to ~3 nm at 3000 eV [*Lindau, 1974*]. The wide variation in (at different incident energies may reflect variations in the deposition rate due to changing operating vacuum and surface contamination conditions for different time profiles, variations in electron current density, or changes in electron stimulated adsorption rate with energy. Carbon deposition rate has been found to vary with vacuum level and partial pressures of organic residual gasses [*Brandis, 1971*]. The deposition rate for this process is known to be approximately linearly proportional to the incident current density and less dependent on beam energy over the range of energies used in this study [*Muller, 1971*].

Initial electron bombardment rapidly removes weakly bound surface contaminants [*Davies, 1997*], through a well-documented process known as electron stimulated desorption [*Ramsier, 1991*]. Although Au is a relatively inert surface, OH^- and H_2O are known to weakly adsorb to Au surfaces; these species are present within the UHV chamber. Figure 2(b) shows a detail of the early time evolution of the SE yield for an incident energy of 1500 eV, with the contribution attributed to term (i) shown as the difference between the solid and dashed lines; the fitting parameters obtained for this curve are listed in Table 1. The inverse of the average removal rate " was 14"7 min for the range of energies studied. Not all time profiles exhibited significant amounts of weakly bound contamination, indicative of varying initial contamination conditions.

As should be expected, there was no evidence of removal of contaminants chemically bound to the inert Au surface, in contrast to removal of Al_2O_3 observed during our initial study [*Davies, 1977*]. Hence, B of term (ii) in Eq. 1 is set to zero.

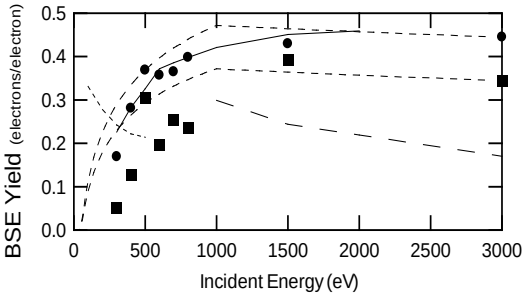

Figure 5. BSE emission curves of Au as a function of incident energy for electron beam exposures of 0 hr (circles) and 60 hrs (squares). Data are taken from Fig. 3. The short dashed lines are fits to Eq. 4 for 0 hr and 60 hr data with Z_{eff} equal to 49.5 and 28.6, respectively. For comparison, lines show yield curves for clean Au [*Thomas, 1970*] (solid) and microcrystalline graphite [*Farhana, 1993* and *Darlington, 1972*] (dotted and long

Yield Curves as a Function of Exposure Time

The data shown in Figs. 2(a) and 3 can be rearranged to produce SE and BSE yield curves at successive elapsed times as shown in Figs. 4 and 5. Inherent in this rearrangement is the assumption that contamination character and rates are consistent for each incident energy deposition curve. While this is not strictly true, as discussed above, it is a reasonable assumption within the limits of the present study.

As can be seen in Fig. 4, the initial SE yield curve at 0 hrs is in very good agreement with our data for clean Au and those of Thomas and Pattinson shown in Fig. 1(a). As the deposition time increases, the trends are for the maximum yield and the peak energy to decrease. At long exposure times, the measured curves are in reasonable agreement with those from disordered carbon measured in other studies [*Bruning, 1938*]. Notice at intermediate times there is clear evidence for a superposition of the yield curve from disordered C on that for bulk Au, rather than a gradual shifting of the shape of the curve from that of Au to that of disordered C.

Parameterization of Yield Curves

The SE yield curves of Fig. 4 can be parameterized in NASCAP in terms of six parameters, as follows. The basic approach for the standard semi-empirical theory of SE emission as a function of incident energy [*Dionne, 1973*] assumes that *(E) may be written as [*Katz, 1977*]

$$\delta(E) = \int_0^R n(E,x)\cdot f(x)\,dx = c_1 \cdot \int_0^R \left|\frac{dE}{dx}\right| \cdot e^{-c_2 \cdot x \cdot \cos(\theta)} dx \qquad (2a)$$

where n(E,x)dx is the average number of SE's produced per incident electron in a layer of thickness dx at depth x below the surface and f(x) is the probability for a SE to migrate to the surface from a depth x and to then escape the surface. Further it is assumed that f(x) is proportional to exp[-$c_2$xcos(2)] and n(E,x) is proportional to the average incident electron energy loss per unit path length (or stopping power), dE/dx. The constants c_2 (the inverse of the SE mean free path) and c_1 (a collection of proportionality constants) can be evaluated in terms of *$_{max}$ and $E_{max.}$ In NASCAP, the range of the incident electrons, R, is represented by the sum of two power law terms as

$$R = b_1 \cdot E^{n_1} + b_2 \cdot E^{n_2} \qquad (2b)$$

in terms of the coefficients b_1 and b_2 and power law exponents n_1 and n_2. (Note only b_1/b_2, n_1 and n_2 are independent parameters [*Purvis*].) The stopping power is assumed to be linear in x and given by

$$n(E,x) \propto \left|\frac{dE}{dx}\right| = \left(\frac{dR}{dE}\right)^{-1} + \frac{d^2R}{dE^2}\cdot\left(\frac{dR}{dE}\right)^{-3} \cdot x \qquad (2c)$$

Standard semi-empirical theory assumes the range is proportional to a single power law (*i.e.*, b_1=0) and that the stopping power is constant for all depths (independent of the second term in Eq. 2c). In this case, Eq. 2a for normal incidence (*i.e.*, 2=0) reduces to

$$\delta_{NAS}(E;E_{\max},\delta_{\max},n_2) = c_1' \cdot \delta_{\max} \cdot \left(E_{\max}/E\right)^{n_2-1} \cdot \left\{1-\exp\left[-c_2' \cdot \left(E/E_{\max}\right)^{n_2}\right]\right\} \qquad (2d)$$

The constants c_2' and c_1' can be evaluated in terms of n_2, independent of the parameters b_1, b_2 and n_1. A number of investigators have proposed variations on the standard semi-empirical theory with different values for 1#n_2#2, including Whiddington's law [*Baroody, 1950*] (n_2=2), Seiler *[Seiler, 1983; Reimer, 1993]* (n_2=1.8), Lane and Zaffarano [*1954*] (n_2=1.66), and Young [*1956*] (n_2=1.35).

Our analysis was performed using n_2=1.35 for three reasons: (i) this is in agreement with Young's work, which is perhaps the most widely accepted semi-empirical model; (ii) the range data for Au has been shown to fit a single power law range equation with n_2=1.31 [*Reimer, 1993 and references therein*], and (iii) as shown below, smaller values of the exponent lead to less severe charging, making the choice of n_2=1.35 the most conservative choice. (Note: This is implemented in NASCAP by setting b_1nb_2 and n_1n1. The independent parameters are *$_{max}$, E_{max} and n_2,)

An alternate model of *(E) at normal incidence, included here for comparison, is the Sternglass [*1954*]

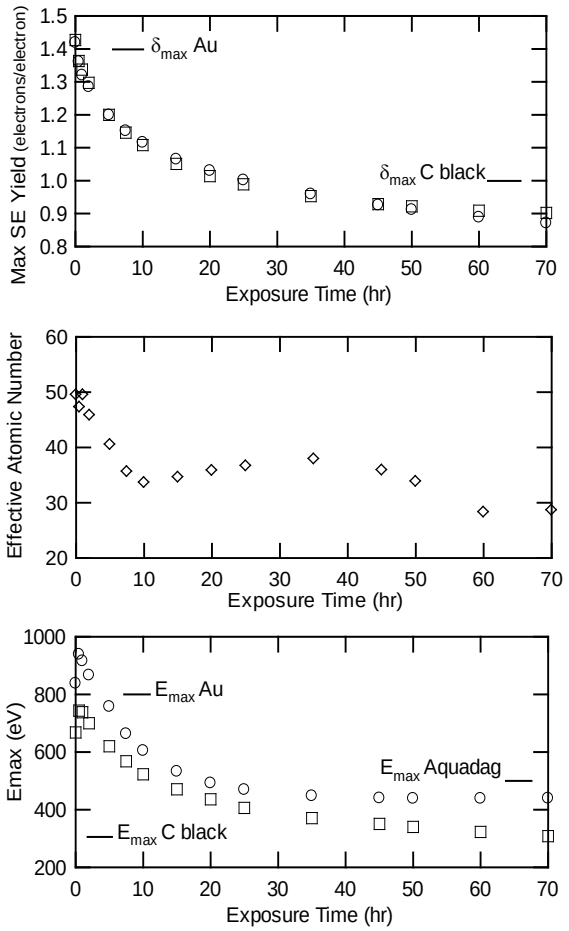

Figure 6. (a) Maximum SE yield δ_{max} and (b) the incident energy, E_{max}, for which δ_{max} occurs, as a function of the exposure time to the electron beam for Au, determined using the NASCAP model of Eq. 2 [*Katz, 1977*] (squares) and the Sternglass model of Eq. 3 [*1957*] (circles). Note the values of δ_{max} and E_{max}, for Au [*Thomas, 1970*], carbon black [*Bruning, 1938*], and microcrystalline graphite [*Bruning, 1938*] indicated. (c) The effective atomic number Z_{eff} as a function of exposure time determined by fitting our data to Eq. 4 for $\eta_o(Z_{eff})$.

model based on the Bethe law for the rate of energy loss in Eq. (2a):

$$\delta_{Stern}(E) = \delta_{\max} \cdot \left(\frac{E}{E_{\max}}\right) \cdot \exp\left[2 - 2\sqrt{E / E_{\max}}\right] \tag{3}$$

The BSE yield curves for exposure times of 0 hr and 60 hrs in Fig. 5 can be parameterized in NASCAP in terms of an effective atomic number Z_{eff}, as shown in Fig. 6(c). The BSE yield for normal incidence at high energies (above ~10 keV), η_o, has a constant value [*Burke, 1977; Darlington, 1972*] given in terms of Z_{eff} by the relation [*Katz, 1977]*

$$0.474 \cdot Z_{eff}^{\,0.177} - 0.4 = 2 \cdot \frac{\left[1 - \eta_o(Z_{eff}) \cdot \left(1 - \ln\left(\eta_o(Z_{eff})\right)\right)\right]}{\left[\ln\left(\eta_o(Z_{eff})\right)\right]^2} \tag{4a}$$

while the BSE yield as a function of incident energy is given by [*Katz, 1977*]

$$\eta(E; Z_{eff}) = \left\{\left[\frac{\log(E/0.05)}{\log(1/0.05)} \cdot \Theta(E - 0.05) \cdot \Theta(1.0 - E)\right] + \Theta(E - 1.0)\right\} \times \left[0.1 \cdot \exp(-E/5) + \eta_o(Z_{eff})\right] \tag{4b}$$

where E is in keV.

NASCAP Parameterization of Yield Curves as a Function of Contamination

Measurements of δ(E) and η(E) at various contamination exposure times (shown in Figs. 4 and 5, respectively) allow determination of the time evolution of the maximum SE yield $\delta_{max}(t)$ and the incident energy, $E_{max}(t)$ for which δ_{max} occurs, together with the effective atomic number $Z_{eff}(t)$. These three parameters (together with exponent in the stopping power that remains fixed at a value of n_2=1.35) are used in the NASCAP code to model the charging of spacecraft in the near earth orbit plasma environment that results from SE and BSE emission [*NASCAP, 1999; Mandell, 1993; Katz, 1977*]. Figure 6 shows the time evolution of the three parameters determined by fitting the data in Figs. 4 and 5 with the NASCAP Eqs. 2 and 4, respectively.

As was seen in Fig. 4, the two parameters characterizing δ(E) change continuously from values very near those of clean Au at 0 hrs to values representative of disordered carbon (between those of carbon black and Aquadag [*Bruning, 1938*]) at 70 hrs. Values of δ_{max} obtained by fits to the NASCAP (Eq. 2) and Sternglass (Eq. 3) models of δ(E) are nearly identical and correspond to the maximum SE yield [see Fig. 6(a)]. The values of E_{max} obtained using the NASCAP model are ~20% less than those for the Sternglass model [see Fig. 6(b)], reflecting the poor fit at higher energies using the Sternglass model [see Fig. 1(a)].

The measured initial BSE yield curve (see Fig. 5) is in excellent agreement with that measured for clean Au by Thomas and Pattinson. At long exposure time, the BSE yield curve has been reduced in magnitude by up to ~25% while maintaining approximately the same shape. Fits to these data using Eq. 4 are shown in the

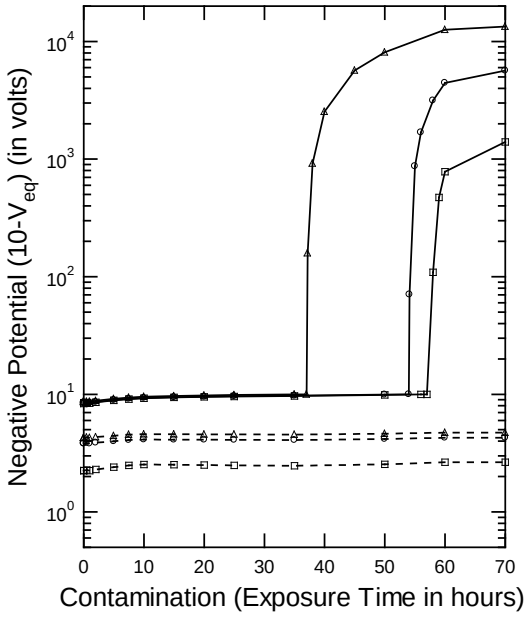

Figure 7. Equilibrium charging potential for a single material using the time evolution of the secondary electron emission parameters for contaminated gold. Curves are for the 4 September, 1997 (squares), worst case (circles), and ATS-6 (triangles) geosynchronous environments in full sunlight (dashed curves) and eclipse (solid curves) [*NASCAP, 1999*].

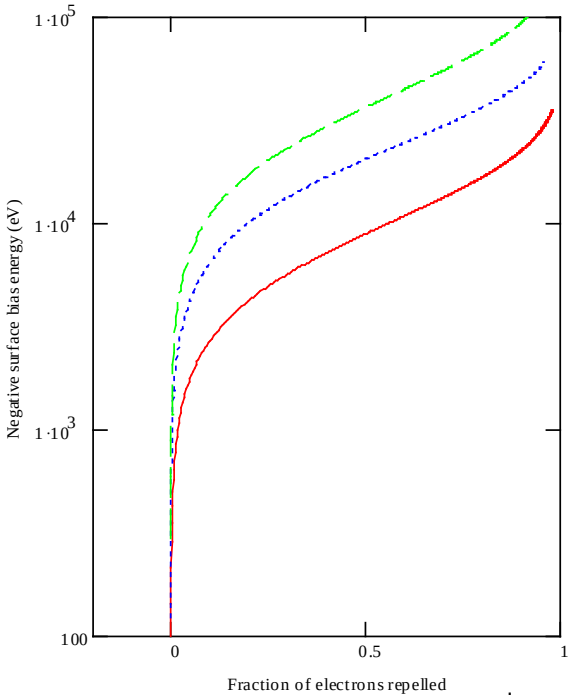

Figure 8. Negative bias of surface for which some fraction of incident electrons are repelled from the surface. Curves are for the 4 September, 1997 (solid), worst case (dotted), and ATS-6 (dashed) geosynchronous environments in eclipse [*NASCAP, 1999*].

figure. Two curves for disordered C are also shown in Fig. 5; both curves exhibit an increase in yield with decreasing incident energy, in contrast to the Au curve. There is clearly little, if any, evidence of C in the long exposure BSE yield curve. This is a clear indication that the thickness of the deposited C film is less than the inelastic electron mean free path. Figure 6(c) shows a trend of decreasing Z_{eff} with increased contamination. The magnitude of Z_{eff} is reduced ~40% over the range of exposure times.

MODELING OF SPACECRAFT CHARGING

Using the three parameters in Fig. 6 to describe the evolution of the secondary electron emission of a Au surface as it becomes contaminated, we have modeled the absolute charging behavior of a hypothetical 1 m x 1 m satellite panel composed of Au as it undergoes environmentally-induced surface modification and concomitant changes in spacecraft charging. Modeling was done using the most current version of the NASCAP Interactive Spacecraft Charging Handbook [*NASCAP, 1999*]. NASCAP default values for Au were used for all materials parameters except those six related to SE and BSE emission. Three representative geosynchronous orbit environments incorporated into NASCAP were considered: (i) a "standard day" of 4 September 1997 (bi-Maxwellian electron distribution with n_1=3.00×10^5 m^{-3}, 2_1=4000 eV, n2=2.00×10^5 m^{-3}, and 2_2=7000 eV); (ii) a typical "worst case" environment (Maxwellian electron distribution with n_1=1.12×10^6 m^{-3} and 2_1=12000 eV) [*Purvis, 1984*]; and (iii) an extreme environment encountered by the Advanced Technology Satellite-6 (bi-Maxwellian electron distribution with n_1=1.22×10^6 m^{-3}, 2_1=16000 eV, n_2=2.36×10^5 m^{-3}, and 2_2=29500 eV). Full sunlight and full shade (eclipse) were also considered, in effect turning on and off the photo-induced electron emission.

Figure 7 shows the equilibrium absolute charging potential for the Au panel as it becomes contaminated. For all cases considered, the satellite panel in full sunlight charges positively, to values ranging from +6 V to + 9V, and is reduced by less than 10% as the surface becomes contaminated. However, in eclipse at a threshold level of contamination, the Au panel undergoes a rapid change, charging from less than +1V to thousands of volts negative bias. The changes in absolute potential vary abruptly as the contamination progresses, but do not exhibit discontinuous behavior.

DISCUSSION

The behavior exhibited in Fig. 7 can readily be understood in terms of the energy distribution of the electrons in the plasma environment, the SE and BSE yields as functions of incident energy, the energy distribution of emitted SE electrons, and the effects of charging on electron emission.

In sunlight, photoelectron emission is dominant, causing an accumulation of positive charge on the surface. The positively biased surface recaptures low energy SE and photoelectrons; because the emission energy distribution of SE is peaked at ~5 eV, in most cases there are sufficient return electrons to limit the positive equilibrium bias to . 10 V [*Nickles, 2000*]. In eclipse, there is no photoelectron emission; however, for most clean metal surfaces there are still sufficient net electron- and ion-induced electron emission to maintain a positive bias [*Olsen, 1982*]. This is the case for low levels of contamination (early times) in eclipse, as shown in Fig. 7.

The scenario is true as long as the total electron yield, $\sigma_{tot} \equiv \delta + \eta + \sigma_{ion}$ remains greater than unity. (F_{ion} is the yield due to ion-induced emission.) However, once $F_{tot}<1$, there are more electron impinging on the surface than leaving, which leads to a net negative charging. Low energy electrons are no longer recaptured by the surface, but are rather repelled by the negatively biased surface. Since negative bias does not significantly affect the SE and BSE yields at lower biases [*Nickles, 2000; Davies, 2000a; Davies, 2000b*], charge can accumulate rapidly, leading to abrupt increases in negative charge accumulation. (F_{ion} is affected by negative charging since ions are attracted to the negative bias surface. However, F_{ion} usually has a much smaller contribution to F_{tot} than * and 0.) It is only when the bias potential reaches sufficiently high values to significantly inhibit the number of primary electrons from the plasma reaching the surface that this rapid accumulation of charge is slowed [*Nickles, 2000*].

This effect of negative bias is illustrated in Fig. 8 for the electron plasma distributions of the three geosynchronous environments considered here. The similarity to the solid curves in Fig. 7 is noteworthy. Since the absolute number of SE and BSE emitted is also reduced with increasing contamination, the solid curves in Fig. 7 should level off faster above the threshold than the curves in Fig. 8, as is observed.

Several mechanisms can act to reduce F_{tot} below unity, resulting in this marked change in the spacecraft equilibrium potential. These include:

(i) An increase in the electron plasma temperature shifts the Maxwellian distribution of the incident primary electrons to higher energies and diminishing the number of low energy electrons below the crossover energy. * decreases above E_{max} (typically above a few hundred volts). 0 also typically decreases above a few thousand volts incident energy until it reaches a plateau at ~10 keV [*Shimizu, 1974*]. Thus, increasing the electron plasma temperature from a few thousand volts upward acts to decrease both * and 0, leading to a threshold charging effect [*Rubin, 1978*]. In the cases studied here, this threshold occurs at an electron plasma temperature of ~11 keV. This is in excellent agreement with the detailed investigation of Olsen, who found a critical transition energy of ~10 keV through modeling and the observed threshold for charging events on ATS-6 and SCATHA satellites above a threshold energy of ~15 keV [*Olsen, 1983*].

(ii) Increases in the electron plasma density enhance the negative charge accumulation due to SE and BSE emission. Thus, increased electron plasma density, particularly at higher energies where SE and BSE yields are lower, enhances the likelihood of the large negative bias threshold effect for a given spacecraft, as was observed by Olsen [*1983*]. By contrast, increases in the electron

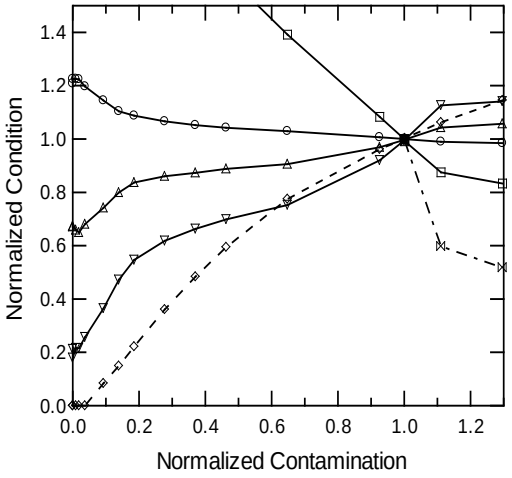

Figure 9. Effects of parameters for environmental conditions and electron emission of materials in terms of contamination. Conditions under study are: □-maximum temperature of Maxwellian electron distribution; ®-electron density; ○-power law exponent for SE distribution; Î- *$_{max}$ of SE yield curve; Ì-E_{max} of SE yield curve; and •-Z_{eff} of BSE yield curve. Conditions and contamination are normalized by dividing by the nominal conditions for the worst case environment for emission parameters at the transition between positive and negative bias shown in Fig. 7.

plasma density have little effect on positively biased surfaces, as a result of the self-regulating nature of positive biasing [*Nickles, 2000*]

(iii) A reduction in the total SE yield, or equivalently in δ_{max}, reduces F_{tot}.

(iv) A reduction in E_{max} means that fewer SE are emitted in a given environment since the number of incident electrons is smaller from the lower energy tail of plasma electron energy distribution.

(v) An increase in the stopping power exponent reduces the SE yield, particularly in the higher energy tail of the yield curve.

(vi) A reduction in total BSE yield also reduces F_{tot}. Recall that from Eq. 4 used by NASCAP to model 0, this corresponds to a reduction in Z_{eff}.

These six mechanisms can be further understood by investigating their effects using the NASCAP modeling code. Figure 9 shows the effect of each mechanism on the threshold for negative charging modeled through the corresponding NASCAP parameter. At each of the contamination values considered in Fig. 7 for the worst case environment all six NASCAP parameters, save one, are fixed at their values for a given contamination; subsequently, each of the six parameters are perturbed from their nominal value at the threshold level of contamination in Fig. 7 for the worst case environment to cause a transition in charging sign. Areas on the graph to the right of the lines indicate conditions for negative bias and to the left of the lines indicate positive bias.

Each parameter exhibits the expected trends discussed above. Negative charging becomes less extreme and the amount of contamination required for the onset of negative biasing increases as the effective temperature of the electron distribution is reduced. As the electron density is reduced, the negative charging becomes less severe. Below the nominal contamination level, no amount of electron density is sufficient to cause negative charging, since all electrons act to positively charge the surface. As either δ_{max} or E_{max} decrease, the negative charging becomes more extreme. Increases in the power law exponent reduce the yield at higher energies, thereby enhancing negative charging; negative charging was found not to occur in any environment studied at $n_2<1.325$. Reduction in Z_{eff} results in enhanced negative charging.

Further, the relative effect of each parameter on the threshold can be determined by examining Fig. 9; smaller magnitude of the slope of the lines correspond to higher sensitivity of the parameter on the threshold energy. Thus, the parameters, ranked in approximate order of increasing sensitivity are electron plasma density, maximum effective temperature of the electron plasma distribution, effective atomic number, E_{max}, δ_{max}, and power law exponent for the SE distribution. Stated another way, the SE yield, the BSE yield, and then the environmental conditions of the electron plasma distribution have the most pronounce effect on the threshold level required for negative charging in geosynchronous environments in eclipse.

CONCLUSIONS

The first two mechanisms that can reduce F_{tot} below unity, listed above, are driven by temporal changes in the plasma environment that can result from convection of stable plasmas populations past the satellite, motion of the satellite with respect to magnetospheric convection boundaries, or injection of hot plasmas by substorms. As noted, these effects have been observed and are discussed by Olsen [*1983*].

This study provides an example where temporal changes in the satellite itself, rather than the spacecraft environment, can lead to a threshold effect for spacecraft charging. As shown above, the contamination of Au lead to the occurrence of mechanisms (iii), (iv) and (vi) for the reduction of F_{tot} and can thus lead to severe negative charging as shown by our modeling. In this case (at least), the threshold for large negative charging in geosynchronous orbits in eclipse are more sensitive to changes in the satellite than to changes in the environment.

The implication of this conclusion for real satellites is obvious and ominous. In many cases, it may not be sufficient to model spacecraft charging of only pristine surfaces during the design phase of satellite development. Modest surface modifications can lead to significant changes in the SE and BSE emission of spacecraft surfaces. In geosynchronous environments, eclipsed surfaces can see dramatic changes in absolute charging and develop kilovolt negative biases. Of particular concern is the possibility of large differential charging between contaminated and uncontaminated surfaces that develop as the secondary electron emission of surfaces evolve due to contamination.

ACKNOWLEDGMENTS

This work was supported by the NASA Space Environment Effects program and in part by the NASA Graduate Student Research Program (Davies). We are grateful to acknowledge Myron Mandell and Ira Katz of Maxwell Technologies for providing us with the latest version of NASCAP and their assistance with its use and interpretation of the modeling results.

REFERENCES

Baroody, E.M., Phys. Rev. 78, 780 (1950).

Brandis, E.K., F.W. Anderson and R. Hoover, in: *Scanning Electron Microscopy 1971*, (IITRI, Chicago, 1971). pp. 505-510.

Brunnig, H. Phiilips Tech. Rev. 3, 80 (1938).

Burke, E.A., "Soft X-ray Induced Electron Emission," IEEE Trans. on Nuclear Sci., NS-24(6), 2505-2511 (19

Chang, W.Y , J.R. Dennsion and Parker Judd, "Measurements of Electronic Properties of Conducting Spacecraft Materials with Application to the Modeling of Spacecraft Charging," Proceedings of the 38th American Institute of Aeronautics and Astronomics on Aerospace Sciences, Reno, NV, January, 12, 2000, in press.

Crutcher, E.R., L. Nishimura, K. Warner, and W. Wascher, Quantification of contaminants associated with LDEF, *LDEF–69 Months in Space, First Post-Retrieval Symposium, NASA Conf. Pub. 3134, pt. 1*,141-147, 1991a.

Crutcher, E.R., L. Nishimura, K. Warner, and w. Wascher, Migration and generation of contaminants from launch through recovery: LDEF case history,, *LDEF–69 Months in Space, First Post-Retrieval Symposium, NASA Conf. Pub. 3134, pt. 1*,121-140, 1991b.

Darlington, E.H. and V.E. Gosslett, "Backscattering of 0.5-10keV electrons from solid targets," J. Phys. D: Appl. Phys. 5 1969-1981 (1972).

Davies, R.E and J.R. Dennison, "The effect of contamination of spacecraft surfaces on secondary electron energy spectra," in preparation, 2000a.

Davies, R.E. and J.R. Dennison, " The effect of negative bias on secondary electron emission from spacecraft surfaces," in preparation, 2000b.

Davies, R.E., "Measurement of Angle-Resolved Secondary Electron Spectra," PhD Thesis, Utah State Univ., 1999.

Davies, R.E., and J.R. Dennison, Evolution of secondary electron emission characteristics of spacecraft surfaces, *J. Spacecraft and Rockets*, 34, 4, 571-574, 1997.

Davies, R.E., An instrument for experimental secondary electron emission investigations, with application to the spacecraft charging problem, *M.S. Thesis, Dept. of Physics, Utah State Univ., Logan, UT*, 1996.

Dennison, J.R, M. Holtz, and G. Swain, "Raman spectroscopy of carbon materials," Spectroscopy, 11(8), 38-46 (1996).

Dennison, J.R., "(e,2e) spectroscopic investigations of the spectral momentum density of carbon films," PhD Thesis, Virginia Tech, 1985.

Dionne, G.F., "Effects of Secondary Electron Scattering on Secondary Emission Yield Curves," J. Appl. Phys. 44(12), 5361 (1973).

Farhang, H., E. Napchant and B.H. Blott, "Electron backscattering and secondary electron emission from carbon targets: comparison of experimental result with Monte Carlo simulations," J. Phys. D: Appl. Phys. 26, 2266-2271 (1993).

Garrett, H.B., The charging of spacecraft surfaces, *Rev. of Geophys. and Space Phys*., 19, 4, 577-616, 1981.

Garrett, H.B., AFGL-TR-78-0116, Air Force Geophysical Laboratory, Hanscom Air Force Base, MA, 1978.

Hardy, D.A., M.S. Gussenhoven, and E. Holeman, A statistical model of auroral electron precipitation, *J. Geophys. Res.*, 90, A5, 4229-4248, (1985).

Hastings, D. and Garrett, H., Spacecraft-environment Interactions, (Cambridge University Press, Cambridge, 1996).

Herr, J.L. and McCollum, M.B.: "Spacecraft Environments Interactions: Protecting Against the Effects of Spacecraft Charging." NASA Reference Publication 1354, NASA Marshall Space Flight Center, November 1994.

Hiller, J., "On the Investigation of Specimen Contamination in the Electron Microscope," *J. Appl. Physics*, 18, 226-230 (1948).

Hren, J.J., *Ultramicrosc*. 3, 375 (1979).

Katz, I., M. Mandell, G. Jongeward, and M.S. Gussenhoven, The importance of accurate secondary electron yields in modeling spacecraft charging, *J. Geophys. Res.*, 91, A12, 13,739-13,744, 1986.

Katz, I.M, D.E. Parks, M.J. Mandell, J.M. Harvey, D.H. Brownwell, Jr., S.S. Wang and M. Rotenberg, "A Three Dimensional Study of Electrostatic Charging in Materials," *NASA CR-135256* (NASA, Greenbelt, MD, 1977).

Lane, R.O, and Zaffarano, "Transmission of 0-40 keV Electrons by Thin Films with Application to Beta-Ray Spectroscopy,"Phys. Rev. 94, 960 (1954).

Leach, R.D. and M.B. Alexander, "Failures and Anomalies Attributed to Spacecraft Charging," NASA Ref. Pub. 1375, Marshall Space Flight Center, 1995

Lindau, I and W.E. Spicer, J. Electron Spectrosc. Relat. Phenom. 3, 409 (1974).

Mandell, M.J., P.R. Stannard and I. Katz, "NASCAP Programmer's Reference Manual," NASA Lewis Research Center, May 1993.

Muller, K.H., *Optik*, 33, 296 (1977).

NASCAP Intreactive Spacecraft Charging Handbook, Beta Version 2.0, (Maxwell Technologies, San Diego , CA, September, 1999.)

Nickles, N. R.E. Davies and J.R. Dennison, "Applications of secondary electron energy- and angular-distributions to spacecraft charging," Proceedings of the 38th American Institute of Aeronautics and Astronomics on Aerospace Sciences, Reno, NV, January, 12, 2000, in press.

Olsen, R.C., A Threshold Effect for Spacecraft Charging, *J. Geophys. Res.*, 88, 493-499, (1983).

Olsen R.C., "The hidden population of the magnetosphere," J. Geophys. Res. 87, 3481-3488 (1982).

Purvis, C.K. H.B. Garrett, A.C. Whittlesey, and N.J. Stevens, *Design Guidelines for Assessing and Controlling Spacecraft Charging Effects*, NASA TP 2361, 1984.

Purvis, private communications.

Ramsier, R.D., and Yates, J.T., Jr., Electron-Stimulated Desorption: Principles and Applications," *Surf. Sci. Rep.* 12(6-8), 247-378 (1991).

Reimer, L., *Image Formation in Low-Voltage Scanning Electron Microscopy*, (SPIE Optical Engineering Press, Bellingham, WA, 1993)Reimer, L. *Scanning Electron Microscopy*, (Springer-Verlag, Berlin, 1985).

Rubin, A.G., P.L. Rothwell and G.K. Yates, "Reduction of spacecraft charging using highly emissive surface materials, in Proceedings of the 1978 Symposium on the Effects of the Ionosphere on Space and Terrestrial

Systems, ed. J.H. Goodman, (Naval Research Laboratory, Washington, D.C. 1978), 313-316.

Shimizu, R. “Secondary electron yield with primary electron beam of kilo-electron-volts,” J. Appl. Phys. 45, 2107 (1974).

Smith, T., “Auger Electron Spectroscopy and Ion Sputter Profiles of Oxides on Aluminum,” *Surf. Sci*., 55(2), 601-624 (1976).

Sternglass, E.J., ”Backscattering of kilovolt electrons from solids,” Phys. Rev., 95, 345-358 (1954).

Sternglass, E.J., “Theory of secondary electron emission by high-speed ions,” Phys. Rev. 108, 1-12 (1957).

Thomas, S., and Pattinson, E.B. “Range of Electrons and Contribution of Backscattered Electrons in Secondary Electron Production in Aluminum,” Journal of Physics D: Applied Physics, 3(3), 349 (1970).

Tong, J.T.L., ed., *Electron Beam Testing Technology*, (Plenum Press, New York, 1993).

Ura, K., “Electron Beam Interactions with Specimen,” in *Electron Beam Testing Technology*, ed. J.T.L. Thong (Plenum Press, New York, 1993).

van Oostrom, A., “Some Aspects of Auger Microanalysis,” *Surf. Sci.*, 89(1-3), 615-634 (1979).

Young, J.R. “Penetration of Electrons and Ions in Aluminum,” J. Appl. Phys., 27, 1 (1956); “Penetration of Electrons in Aluminum Oxide Films,” Phys. Rev. 103, 292 (1956).